Cancer Biol Med 2019. doi: 10.20892/j.issn.2095-3941.2019.0073

ORIGINAL ARTICLE

OPEN ACCESS

Downregulation of KCTD12 contributes to melanoma stemness by modulating CD271

Weiyu Shen[1*], Yumei Li[1*], Bifei Li[1], Liping Zheng[2], Xiaodong Xie[1], Jingqing Le[1], Yusheng Lu[3], Tao Li[1], Fan Chen[1], Lee Jia[1,3]

[1]Cancer Metastasis Alert and Prevention Center, College of Chemistry and Fujian Provincial Key Laboratory of Cancer Metastasis Chemoprevention and Chemotherapy, Fuzhou University, Fuzhou 350108, China; [2]Department of Pharmacy, Fujian Provincial Maternity and Children's Hospital, Fuzhou 350001, China; [3]Institute of Oceanography, Minjiang University, Fuzhou 350108, China

ABSTRACT

Objective: Cancer metastasis remains the primary cause of cancer-related death worldwide. In a previous study, we found that levels of BTB/POZ domain-containing protein KCTD12 are lower in metastatic melanoma cells than in parental melanoma cells. The purpose of this study was to identify the roles of KCTD12 in cancer metastasis.

Methods: The Cancer Genome Atlas (TCGA) datasets were used to evaluate the relationship between KCTD12 and skin cutaneous melanoma (SKCM) prognosis. The effects of endogenous KCTD12 on biological behaviors were examined using the MTT assay. The impacts of KCTD12 on melanoma stemness were explored using spheroid formation assay. KCTD12 knockout A375 cells were generated to confirm the inhibitory effect of KCTD12 on CD271, and a mouse metastatic model was used to determine the impact of KCTD12 on melanoma metastasis *in vivo*.

Results: KCTD12 levels were lower in lung metastatic cells than in paired parental melanoma cells, and low KCTD12 expression indicated a poor prognosis in SKCM. Cancer metastasis-related capacities were higher in lung metastatic cells than in parental melanoma cells. Moreover, KCTD12 knockdown enhanced tumor growth and metastasis both *in vitro* and *in vivo*. Mechanistically, the interaction between KCTD12 and CD271 might be responsible for the stemness transformation after KCTD12 knockdown.

Conclusions: This study identifies for the first time the role of the interaction between KCTD12 and CD271 in inducing melanoma cell stemness transformation. Moreover, KCTD12 repression enhances melanoma cell growth, adhesion, migration and invasion.

KEYWORDS KCTD12; MITF; CD271; melanoma; cancer metastasis; cancer stem cell

Introduction

The BTB/POZ domain-containing protein KCTD12 (KCTD12), also known as Pfetin, is a membrane protein encoded by the *KCTD12* gene, as well as an auxiliary subunit of GABA-B receptors, which determine the pharmacology and kinetics of the receptor response. KCTD12 has been reported to be a prognostic biomarker of gastrointestinal stromal tumors[1-4]. A previous study reported that colorectal cancer stemness was regulated by KCTD12 through the ERK pathway[5]. Earlier reports declared that KCTD12 promoted the proliferation of human uveal melanoma OCM-1 cells[6]. In addition, it was reported that KCTD12 acted as a tumor suppressor in esophageal squamous cell carcinoma (ESCC) through the WNT/NOTCH pathway and chromatin remodeling[7]. However, the role of KCTD12 in cutaneous melanoma progression has yet to be investigated.

The cancer stem cell (CSC) hypothesis has been proposed for a long time, and it applies to many cancers, such as breast cancer and lung cancer[8-10]. However, its applicability to melanoma is controversial[11-14]. The supporters argue that there are different hierarchies in melanoma, and these classes possess varied tumorigenicity; for example, melanoma stem cells have the strongest tumorigenic ability[15]. Some advocates have shown that melanoma cells can differentiate into multicellular lineages, such as melanocytes, adipocytes and chondrocytes, under suitable conditions[16]. However, the

*These authors contributed equally to this work.
Correspondence to: Lee Jia
E-mail: jiali@fzu.edu.cn
Received February 17, 2019; accepted May 5, 2019.
Available at www.cancerbiomed.org

opponents provide evidence that they cannot find the rare highly oncogenic cell subpopulations[12]. Instead, they have found that the majority of melanoma cells jointly express the so-called stem cell markers, and this does not fit the rarity criterion of the CSC theory. Other opponents have demonstrated that cancer cells possess equal tumorigenicity independent of the level of stem cell markers in some melanoma types. All in all, the CSC hypothesis requires more proof to convince the objectors.

Under normal circumstances, cell differentiation seems to be irreversible in humans. However, increasing evidence suggests that cell differentiation may be reversible in some abnormal situations, such as cancer, and this process is defined as dedifferentiation[17-21]. The reason and mechanism underlying the reversal of differentiation in cancer are far from understood. Even so, many studies have proven that cancer cells, which undergo dedifferentiation, acquire stem cell traits, such as high tumorigenicity and the ability to differentiate again[19,22,23].

CD271, also known as tumor necrosis factor receptor superfamily member 16, is encoded by the *NGFR* gene and is a receptor for neurotrophin and tumor necrosis factor (TNF); CD271 has also been reported as a CSC marker in various cancers[24-28]. Earlier studies revealed that CD271 could enrich the CSCs population in melanoma[24,29]. Despite the great success reported above, to the best of our knowledge, the relationship between KCTD12 and CD271 in melanoma has not been studied until now. In the current study, we show for the first time that KCTD12 downregulation in melanoma altered differentiated melanoma cells to a more immature and highly tumorigenic state through the KCTD12-MITF-CD271 axis. Interestingly, the acquisition of CSC phenotypes induced by KCTD12 inhibition did not occur *via* the well-known epithelial-mesenchymal transition (EMT) pathway.

Materials and methods

Reagents

Anti-CD271 antibody was purchased from Signalway Antibody LLC (Nanjing, China). Anti-KCTD12 antibody was purchased from GeneTex (California, USA). Anti-E-cadherin, anti-N-cadherin, anti-β-actin and goat anti-rabbit lgG H&L antibodies were all from Wanleibio (Shenyang, China). For flow cytometry, anti-CD49a (PE), anti-CD49d (PE), anti-CD133 (PE), and anti-EpCAM (PE) antibodies and mouse IgG1 kappa isotype control antibody (PE) were from BD Biosciences (California, USA) or eBioscience (New York, USA). Goat anti-rabbit IgG(H+L)/Cy3 was purchased from Boster Biological Technology (Wuhan, China). Primers for RT-qPCR were from Sangon Biotech (Shanghai, China), and the sequences are listed in **Supplementary Table S1**. KCTD12-siRNA and negative control siRNA (Ctrl-siRNA) were purchased from Sangon Biotech (Shanghai, China), and the sequences are listed in **Supplementary Table S2**. Small guide RNAs (sgRNAs) were synthesized by TSINGKE Biological Technology (Fuzhou, China). The MITF inhibitor was purchased from MedChem Express (Princeton, NJ, USA).

Lung metastatic cell line establishment and cell culture

The parental B16F10 mouse melanoma and A375 human melanoma cell lines were purchased from the Cell Resource Center of the Shanghai Institute for Biological Sciences (Shanghai, China). The progeny B16F10M cell line was derived from B16F10 cell lung metastasis in C57BL/6 mice employing the experimental metastatic model reported previously[30]. Similarly, the A375M cell line was established from A375 cell lung metastasis in BALB/C nude mice. Procedures for establishing the metastatic cell lines were as follows. Briefly, B16F10 and A375 cells were first transfected with pEGFP-N1 plasmid (4.7 kb, USA) to induce green fluorescent protein (GFP) expression. One month after the cells were injected intravenously into mice, metastatic lesions in the lungs were stripped and washed thoroughly with phosphate buffer solution (PBS). Then, the tumor tissue blocks were cut into pieces and digested with a trypsin (0.1%) and collagenase I (0.1%) mixture. Additional tumor blocks were collected and processed for imaging with a laser scanning confocal microscope (Leica TCS SP8, USA) after co-staining with 4,6-diamino-2-phenylindole (DAPI). Later, the cells were washed with PBS and cultured in complete medium. After the indicated number of days, GFP expression was verified in the established cell lines using a fluorescence microscope (Zeiss, Germany); the cells were co-stained with DAPI to verify that they were from the parental melanoma cells, rather than from the host.

The melanoma cells and lung cancer A549 cells were cultured in RPMI 1640 medium (HyClone, USA) containing 10% (v/v) fetal bovine serum (FBS; Gembio, USA), 1% penicillin/streptomycin and 2 mM glutamine. Colon cancer SW620 cells were cultured in L-15 medium. All the cells were maintained at 37°C in a humidified atmosphere with 5% CO_2. B16F10M cells and A375M cells were used for assays within 5 passages.

RT-qPCR analysis

RT-qPCR analysis was performed as reported previously[31]. Briefly, total RNA extraction and cDNA synthesis were performed using Trizol reagent (Thermo Fish, USA) and a PrimeScript™RT reagent kit (TAKARA, Japan), respectively. Subsequently, quantitative PCR was performed in triplicate using SYBR®Premix Ex Taq™ (TAKARA, Japan). The mRNA levels were normalized to that of *ACTB* using the $2^{-\Delta\Delta Ct}$ method. The PCR products were verified using sodium dodecyl sulfate-polyacrylamide gel electrophoresis (SDS-PAGE) coupled with SYBR Green (**Supplementary Figure S1**).

siRNA-mediated knockdown of KCTD12

B16F10 cells or A375 cells at 70% to 80% confluency in OPTI-MEM (Invitrogen, USA) were transfected with the indicated siRNA duplexes using Lipofectamine 3000 (Invitrogen, USA). After 6 h of incubation, the transfected medium was replaced with complete medium, and cultured for 48 h before further assays. The interference efficiency of KCTD12 was detected by RT-qPCR and Western blot.

MITF inhibitor-mediated knockdown of MITF

In order to find out the relationship between MITF and CD271, ML329, a specific small molecule inhibitor of MITF was employed to repress the expression of MITF in A375 cells. Briefly, A375 cells were incubated with 26 μM ML329 for 24 h, and its effect on MITF and CD271 expression level was measured by RT-qPCR.

Immunoblotting

Immunoblotting was performed as described previously[32]. Briefly, total protein lysates were prepared using a radio-immunoprecipitation assay (RIPA; Beijing Dingguo Changsheng Biotechnology, Beijing, China) lysis buffer supplemented with the protease inhibitor phenylmethanesulfonyl fluoride (PMSF; Beijing Dingguo Changsheng Biotechnology, Beijing, China). Protein concentrations were determined using a BCA kit (Beijing Dingguo Changsheng Biotechnology, Beijing, China). Proteins were separated on SDS-PAGE gels, and transferred onto polyvinylidene difluoride (PVDF) membranes (Bio-Rad, USA). Then, the membranes were probed overnight at 4°C with the following primary antibodies: KCTD-12, CD271, E-cadherin, N-cadherin and β-actin. Next, the membranes were washed with Tris Buffered Saline Tween (TBST), and incubated with the appropriate horseradish peroxidase-conjugated secondary antibodies (Beijing Dingguo Changsheng Biotechnology, Beijing, China). Protein bands were visualized with hypersensitive chemiluminescence kit (Wanleibio, Shenyang, China). Immunodetection was accomplished using the ChemiDoc XRS system (Bio-Rad, USA). Finally, densitometric analyses were performed using ImageLab software (Bio-Rad, USA).

Immunofluorescence

Immunofluorescence assays were conducted as previously reported[33]. Briefly, cells plated on coverslips were fixed with 4% paraformaldehyde for 30 min. After that, they were washed with PBS, and blocked with a 5% goat serum PBS solution for 30 min at room temperature. Next, the cells were incubated with KCTD12 antibody (Santa Cruz, USA) diluted in blocking buffer overnight at 4°C, followed by Cy3-conjugated secondary antibody incubation for 30 min. Afterward, the nuclei were stained with DAPI for 15 min at room temperature. Finally, the stained cells were visualized, and pictures were taken under a laser scanning confocal microscope (Leica TCS SP8, USA) or a fluorescence microscope (Zeiss, Germany).

Flow cytometry

The assay was carried out as per the procedures described previously[34]. All samples were analyzed on a BD FACSAriaIII cell sorter (BD Bioscience, USA). For the membrane protein expression analysis, cells were incubated with the indicated fluorophore-conjugated antibody at 4°C in the dark for 30 min. Then, the indicated channel was used to analyze the fluorescence intensity with an isotype control antibody to exclude false positives. For cell sorting, microballoon beads (BD Bioscience, USA) were employed to calculate the droplet delay. Then, the untreated cells were applied to adjust the signal amplification voltage. Finally, the positive cells were sorted for further assays.

Cell proliferation assay *in vitro*

As described previously[35], a cell proliferation assay was conducted using the methyl thiazolyl tetrazolium (MTT) method. Cells were plated into 96-well plates at a density of

3,000 cells/well and cultured at 37°C in a humidified atmosphere with 5% CO_2. After the indicated time, complete medium was replaced with MTT-containing basal medium without phenol red, and the cells were incubated for another 4 h. Then, the formazan formed by viable cells was completely dissolved in 100 μL dimethyl sulfoxide (DMSO). Cell viability was determined by detecting the absorbance at 490 nm using an Infinite M200 Pro microplate reader (Tecan, Switzerland).

Cytotoxicity assay *in vitro*

According to procedures described previously[31,36,37], the cytotoxicity of doxorubicin (DOX, Dalian Meilun Bio, China) was investigated by MTT assay. Briefly, cells were plated into 96-well plates at a density of 1×10^4 cells/well, and cultured at 37°C in a humidified atmosphere with 5% CO_2. After overnight culture, the cells were treated with different concentrations of DOX for 24 h. The subsequent procedures were the same as the above cell proliferation assay. Culture medium was used as a blank control, and the absorbance of untreated cells was considered 100% viability. Cell viability was computed according to the following equation: Cell viability = $(OD_{treated}/OD_{control}) \times 100\%$. Each sample was assayed in triplicate in three independent experiments.

Cell adhesion assay

Cell adhesion assays to gelatin or HUVECs were carried out as reported with slight modification[38]. Briefly, 24-well culture plates were coated with gelatin or HUVECs. Then, the cells were trypsinized and stained with Rhodamine123. Next, equal numbers of cells (1×10^4 cells/well) were added to the 24-well culture plates and cultured for 1 h. The non-adherent cells were removed from the plate by thorough washing with PBS. Finally, ten visual fields for each well were selected randomly, and images were taken under a fluorescence microscope (Zeiss, Germany).

Colony formation assay

A colony formation assay was carried out based on a previous procedure with minor modification[39]. Cells were plated into a 6-well culture plate (1,000 cells/well), and the medium was replaced every 3 days until the cell colonies were macroscopic. The cell colonies were fixed with 4% paraformaldehyde and then stained with a 0.1% crystal violet solution. Colonies were observed and photographed using a light microscope (Zeiss, Germany), and colonies with > 50 cells/colony were counted.

In vitro migration and invasion assays

As others reported previously[40,41], migration and invasion assays were carried out using a Boyden chamber incubated with or without Matrigel beforehand. Briefly, cells were trypsinized and adjusted to the indicated density. Then, 1×10^5 cells were added into the upper chamber, and 20% FBS medium solution was added to the lower chamber as the chemokine. Cells were cultured in a humidified atmosphere with 5% CO_2 for the indicated times. Then, the cells on the upper chamber were wiped off, and the cells adhering to the other side of the membrane were fixed with a 4% paraformaldehyde and stained with 0.1% crystal violet solution. Finally, the cells on the membrane were photographed under a light microscope (Zeiss, Germany). Ten fields were selected randomly and the cell number was counted for each group. The experiment was conducted in triplicate.

Detection of melanin content and tyrosinase activity

Assays were carried out based on procedures reported previously[39]. The same amount of cells was collected for the detection of melanin content and tyrosinase activity. For melanin content detection, cells were resuspended in a mixture consisting of ethanol and ether for 15 min at room temperature. Then, the suspension was centrifuged, and the sediment was solubilized by treatment with a 1 M NaOH and 10% DMSO mixture for 30 min at 80°C. Finally, the absorbance was recorded at 470 nm using an Infinite M200 Pro microplate reader (Tecan, Switzerland).

To measure tyrosinase activity, the cell precipitates described above were treated with 0.5% sodium deoxycholate in an ice-water bath for 15 min. Then, 0.1% L-dopa was added to the mixture and incubated at 37°C. The absorbance at 475 nm was detected after the mixture reacting for 0 min and 10 min using an Infinite M200 Pro microplate reader (Tecan, Switzerland). The tyrosinase activity was calculated according to the following equation: tyrosinase activity = $(A_{10\ min} - A_{0\ min})$/cell number.

Bioinformatic analyses

Human SKCM data were extracted from the TCGA database,

and graphics were drawn using the online Gene Expression Profiling Interactive Analysis (GEPIA; http://gepia.cancer-pku.cn/index.html) database[42]. Survival curves were estimated with the Kaplan-Meier method and compared by log-rank test. *KCTD12* transcription was normalized to that of *ACTB*, and the cutoff for high expression and low expression KCTD12 was determined according to the median KCTD12 expression.

Targeted CRISPR/Cas9 KCTD12-KO mutant A375 cell line

sgRNAs (sense: 5'-CACCGCGTGGATTACCCAACGGGGG-3'; anti-sense: 5'-AAACCCCCCGTTGGGTAATCCACGC-3') were designed on the website (http://crispr.mit.edu/) supported by Zhang's lab (**Supplementary Figure S2**). The Cas-OFFinder website (http://www.rgenome.net/cas-offinder) was used to predict the off-target effects. The assay was conducted as per the methods described by Zhang with few changes[43]. Briefly, the construction of the vectors was as follows. First, the PX458 plasmid (Micro Helix, Beijing, China), which contained an eGFP tag, was enzyme digested by the BbsI-HF restriction endonuclease (New England Biolabs, USA). Second, the annealed double strand sgRNA was connected to the open-loop PX458 plasmid. Then, the constructed vector was purified, transformed into the competent DH5α Escherichia coli, and amplified under ampicillin pressure. Before the vector was extracted from Escherichia coli using an endotoxin-free plasmid extraction kit (Solarbio, China), it was sent for sequencing (Sangon, Shanghai, China). Then, the vector was transfected into the indicated melanoma cells using Lipofectamine 3000 (Thermo, USA) according to the manufacturer's instructions. Lastly, the GFP-positive melanoma cells were sorted using a BD FACSAriaIII cell sorter (BD Bioscience, USA). The knockout of the target gene was verified by Western blot.

Apoptosis detection with a calcein-AM/PI kit

Apoptosis was detected using a calcein-AM/PI kit (BestBio Science, Shanghai, China) according to the manufacturer's instructions. Briefly, the treated cells were washed with PBS and stained with calcein-AM at 37°C for 20 min in the dark. Then, the cells were stained with PI for 5 min under the same conditions after being washed with PBS. Finally, images were taken under a fluorescence microscope (Zeiss, Germany) with an excitation wavelength of 488 nm. The viable and apoptotic cells were positive for calcein and PI, respectively, which emitted yellow-green fluorescence and red fluorescence.

Spheroid formation assay

Cells were collected and adjusted to equal concentrations with complete medium. Then, an equal volume of cell suspension was added to a 96-well spheroid microplate (Corning, Wuhan, China). The medium was replaced with fresh complete medium every 2 days. Then, the spheroids were observed, and images were captured under an inverted microscope (Zeiss, Germany) every day. The spheroids were stained with calcein-AM, and images were taken under a fluorescence microscope (Zeiss, Germany) on the indicated day.

Animal experiment

All animal experiments were approved by the Institutional Animal Care and Use Committee of Fuzhou University and operated following the NSFC regulations concerning the care and use of experimental animals. Mice were given access to food and water ad libitum. Unless specified otherwise, all mice were obtained from Fuzhou Wushi Animal Center (Fuzhou, China) and were used at 4–6 weeks of age. To establish B16F10M and A375M cell lines, parental melanoma B16F10 cells and A375 cells were injected into the tail veins of C57BL/6 mice and BALB/C nude mouse, respectively. To determine the effect of KCTD12 expression on *in vivo* metastatic capability, A375 cells before and after KCTD12 knockout with the CRISPR/Cas9 system were injected intravenously into BALB/C nude mice. After approximately 2 months, the mice were euthanized, and the main visceras were collected for further study, such as metastatic node counting and H&E staining. The weights of the mice were determined every three days.

Statistical analysis

All data were analyzed using GraphPad Prism software and are expressed as the mean ± SD. Unpaired Student's *t*-test was applied for comparison between two groups. The log-rank (Mantel-Cox) test was employed for the Kaplan-Meier analysis of overall survival and disease-free survival between low KCTD12 SKCM patients and high KCTD12 SKCM patients. Differences were considered to be significant for $P < 0.05$, and $P < 0.01$ was indicative of highly significant difference.

Results

Lower KCTD12 levels and more aggressive biological behavior in metastatic A375M cells than in parental A375 cells are verified

In our previous study, we established the lung metastatic B16F10M cell line and A375M cell line using an experiment metastatic model (**Supplementary Figure S3**). The fluorescent photographs of tumor tissues and cultured cells were both positive for GFP, which indicated that the tumors and cells were isogenous with the A375-GFP cells injected 2 months before. From our previous proteomics results, we knew that KCTD12, identified by mass spectrum (MS) analysis in Isobaric Tags for Relative and Absolute Quantitation (iTRAQ), was lower in metastatic B16F10M cells than in parental B16F10 cells (**Figure 1G** and **Supplementary Figure S4**; $P < 0.01$). Two characteristic peptides were identified from the KCTD12 protein in the MS analysis.

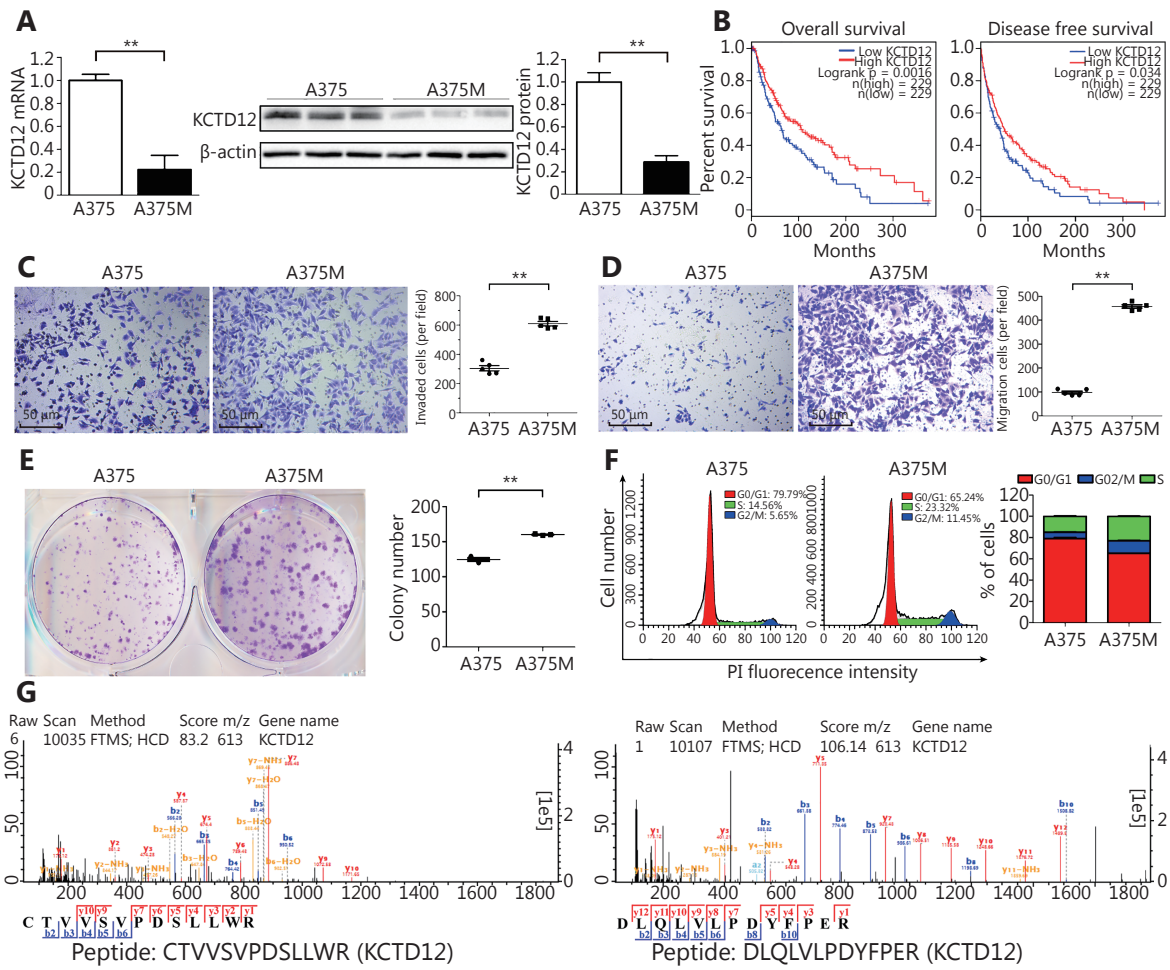

Figure 1 The lower KCTD12 expression and more aggressive biological behavior in A375M cells than in A375 cells. (A) KCTD12 expression was lower in A375M than A375 demonstrated by both RT-qPCR (left panel) and Western blot (middle and right panels). (B) Kaplan-Meier analysis of overall survival and disease free survival in SKCM patients with low (n = 229) and high (n = 229) expression of KCTD12. (C-E) Quantitative analysis showed that A375M exhibited higher invasion (C, 24 h)/ transmigration (D, 24 h)/ colony formation (E, 8 days) abilities than A375. (F) Flow cytometry scans (left panel) and quantitative analysis (right panels) showed that more A375M cells stayed in S and G2/M phases than A375 cells. (G) Mass spectra of characteristic peptides from KCTD12 detected in iTRAQ. Scale bars: 50 μm. Data are mean ± SD (n = 3 - 5); **, $P < 0.01$, determined by one-tailed unpaired t-test; A log-rank test was used to compare the survival curves between low KCTD12 SKCM patients and high KCTD12 SKCM patients.

In this study, we verified KCTD12 downregulation in B16F10M cells compared with B16F10 cells by immunofluorescence (**Supplementary Figure S5**). Naturally, we wondered whether the KCTD12 expression pattern in paired human A375 and A375M cells was consistent with the paired mouse B16F10 and B16F10M cells. Hence, we examined KCTD12 expression in A375 and A375M cells at the mRNA and protein levels. As expected, both the transcriptional and translational levels of KCTD12 were lower in metastatic A375M cells than in parental A375 cells (**Figure 1A**; $P < 0.01$). To evaluate the effect of KCTD12 expression on the clinical prognosis of melanoma, the correlation between KCTD12 expression and the clinical outcomes of patients with SKCM was explored using data from GEPIA (http://gepia.cancer-pku.cn/detail.php). We found that low KCTD12 expression was correlated with poor prognosis in SKCM patients (**Figure 1B**).

To evaluate the proliferative and metastasis-related capacities of A375 and A375M cells, transwell migration, Matrigel invasion, and colony formation assays et al. were carried out. Unless explicitly stated, the same number of cells from different groups was used in these studies. The Matrigel invasion assay results showed that the invasion ability of A375M cells was double that of A375 cells (number of invaded cells: 611 ± 15 per field and 305 ± 18 per field, respectively) (**Figure 1C**; $P < 0.01$). Regarding migratory capacity, the number of migrated cells was 457 ± 7 per field and 98 ± 6 per field for A375M and A375 cells, respectively, which indicated that the mobility of A375M cells was over quadruple that of A375 cells (**Figure 1D**; $P < 0.01$). Next, we examined the proliferative activity of the two cell lines by colony formation assay. The same number of cells (1,000 cells/well) was plated initially, and the colony number was measured 8 days later. The number of colonies formed by A375M cells was higher than that formed by A375 cells (160 ± 1 per well *vs.* 125 ± 3 per well) (**Figure 1E**, right panel; $P < 0.01$). Moreover, the size of colonies formed by the former cells was much larger than that formed by the latter cells (**Figure 1E**, left panel). In addition, cell cycle analysis results showed that significantly more A375M cells than A375 cells (34.74% *vs.* 20.82%) were in S/G2-M phases, which serves as a cell proliferative activity indicator (**Figure 1F**). As shown in **Supplementary Figure S6**, the MTT assay also demonstrated that the proliferative capacity of A375M cells was higher than that of A375 cells. In agreement with our previous results from paired B16F10 and B16F10M cells, A375M cells showed more aggressive biological behavior than A375 cells.

Downregulation of KCTD12 expression induces more aggressive biological behavior in B16F10 cells

To examine whether KCTD12 downregulation played a significant role in the enhanced aggressive biological behavior in B16F10 cells, we employed a siRNA that specifically knocked down KCTD12. KCTD12 knockdown in B16F10 cells was confirmed by RT-qPCR (**Figure 2A**, left panel; $P < 0.05$) and Western blot (**Figure 2A**, middle and right panels; $P < 0.01$). We next examined the effects of KCTD12 knockdown on B16F10 cells through proliferation, adhesion, motility and invasion assays *in vitro*. For the proliferation assay, the same number of cells was plated initially, and cell proliferation was measured 24, 48, 72, 96 and 120 h later. The results showed that KCTD12-suppressed B16F10 cells proliferated observably faster than in the control cells (**Figure 2B**). In the gelatin adhesion assay, slightly more cells in the KCTD12-suppressed group than the control group adhered to the gelatin at 1 h (**Figure 2C**; $P < 0.05$). The improved adhesion capacity was evidenced by the upregulation of integrin alpha 4 (ITGA4; **Supplementary Figure S7**).

Mobility analysis showed that the migratory ability of B16F10 cells increased immensely after KCTD12 knockdown (number of migratory cells: 42 ± 4 per field and 344 ± 15 per field in the ctrl-siRNA and KCTD12-siRNA treated groups, respectively) (**Figure 2D**; $P < 0.01$). In the invasion assay, the number of invaded cells was 82 ± 3 per field and 236 ± 5 per field before and after KCTD12 knockdown in B16F10 cells ($P < 0.01$), which indicated that KCTD12 inhibited the invasion capacity of melanoma cells (**Figure 2E**). The increased invasion ability of KCTD12-knockdown B16F10 cells might be partly attributed to the upregulation of matrix metalloproteinase-9 (*MMP9*; **Figure 4C**, third panel; $P < 0.01$).

KCTD12 downregulation induces more aggressive biological behavior in A375 cells

We next examined whether KCTD12 played an analogical role in melanoma cells originating from humans. KCTD12 knockdown in A375 cells was achieved using the same siRNA used in B16F10 cells because the nucleotide sequence recognized by this siRNA is conserved between humans and mice. KCTD12 knockdown in A375 cells was confirmed by RT-qPCR (**Figure 3A**, left panel; $P < 0.05$) and Western blot (**Figure 3A**, middle and right panel; $P < 0.01$).

Likewise, we examined the effects of KCTD12 knockdown on A375 cell biological behavior *in vitro*. As described above,

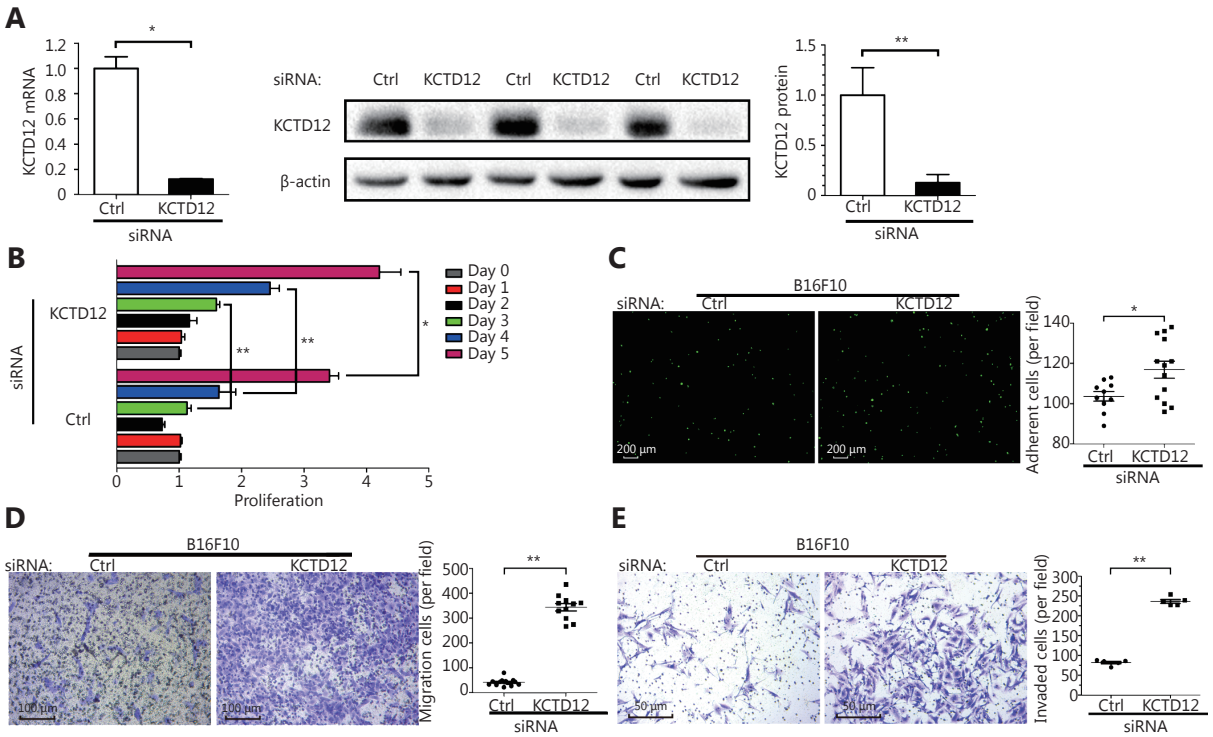

Figure 2 KCTD12 downregulation promotes B16F10 cells' proliferative and metastasis-related capacities. (A) KCTD12 knockdown *via* siRNA in B16F10 cells was confirmed by RT-qPCR (left panel) and Western blot (middle and right panels). (B) Proliferative capacity and (C) heterogeneous adhesion capacity (1 h) of B16F10 cells were enhanced after KCTD12 siRNA treatment. Scale bars: 200 μm. (D) Transmigration capacity and (E) invasion capacity of B16F10 were strengthened after KCTD12 siRNA treatment (72 h). Scale bars: 100 μm for D and 50 μm for E. Data are mean ± SD (n = 3 - 5); *, $P < 0.05$; **, $P < 0.01$, determined by one-tailed unpaired t-test.

the same number of cells (3,000 cells/well) was plated, and cell proliferation activity was measured 24, 48, 72 and 96 h later. KCTD12 knockdown significantly promoted the proliferative capacity of A375 cells (**Figure 3B**). Moreover, the colony formation assay showed that the number of colonies increased significantly from 100 ± 2 per well to 169 ± 9 per well before and after KCTD12 knockdown in A375 cells (**Figure 3C**; $P < 0.01$), which powerfully supported the proliferation assay results described above.

Next, we examined the impact of KCTD12 knockdown on adhesion capacity in A375 cells. A gelatin adhesion assay (**Figure 3D**) and HUVEC adhesion assay (**Figure 3E**) both indicated that KCTD12 knockdown boosted the adhesion capability of A375 cells. Specifically, in the gelatin adhesion assay, the number of adhesive cells increased from 124 ± 4 per field to 144 ± 5 per field before and after KCTD12 knockdown (**Figure 3D**; $P < 0.01$). The corresponding quantitative values for the HUVEC adhesion assay were 194 ± 11 per field and 260 ± 16 per field (**Figure 3E**; $P < 0.01$). Additional evidence for the enhancement of adhesion capacity was the upregulation of adhesion molecules, such as integrin alpha 1 (ITGA1) and epithelial cell adhesion molecule (EpCAM) (**Figure 4E**, third and fourth panel).

Similar to the B16F10 mobility and invasion assay results, KCTD12 knockdown drastically boosted the migratory and invasion abilities of A375 cells (**Figure 3F-3G**). Specifically, the migratory cell number increased from 99 ± 8 per field to 360 ± 8 per field after KCTD12 knockdown in A375 cells (**Figure 3F**; $P < 0.01$). The migration promoting role of KCTD12 downregulation was similar in other cancer cells, such as colon cancer SW620 cells (**Supplementary Figure S8**). In the invasion assay, the number of invaded cells was 305 ± 18 per field and 1060 ± 57 per field before and after KCTD12 knockdown in A375 cells (**Figure 3G**; $P < 0.01$). This result might be explained by the upregulation of the invasion-related gene *MMP9* (**Figure 4E**, first panel; $P < 0.01$). Moreover, the suspension growth A375 cells expressed lower KCTD12 expression than the adherent growth A375 cells, which indicated that the downregulation of KCTD12 endowed A375 cells with anoikis-resistant ability (**Supplementary Figure S9**).

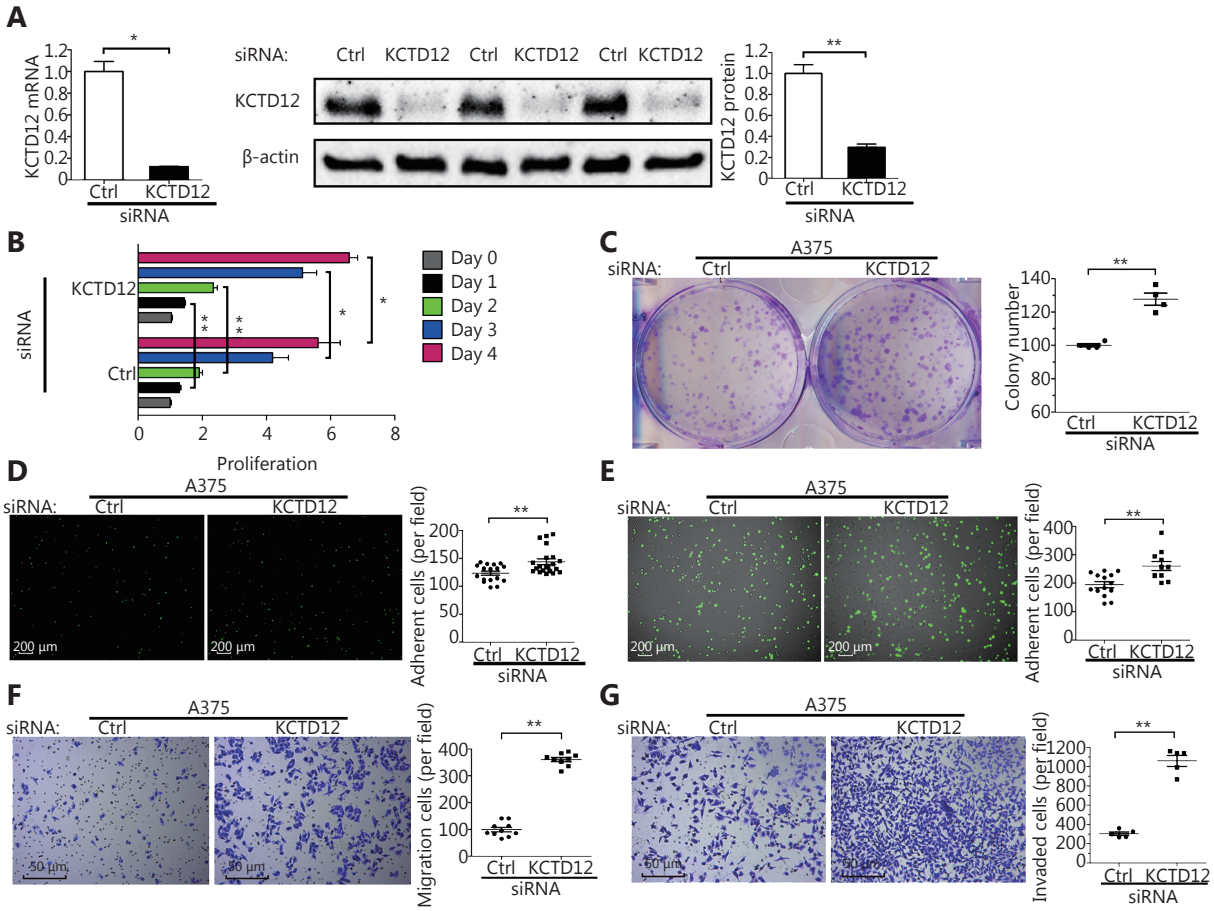

Figure 3 KCTD12 downregulation promotes A375 cells' proliferative and metastasis-related capacities. (A) KCTD12 knockdown *via* siRNA in A375 cells was confirmed by RT-qPCR (left panel) and Western blot (middle and right panels). (B) Proliferative capacity and (C) colony formation capacity (8 days) of A375 cells were enhanced after KCTD12 knockdown. (D) Gelatin adhesion capacity and (E) HUVEC adhesion capacity were increased after KCTD12 knockdown in A375 cells (1 h). Scale bars: 200 μm. (F) Transmigration capacity and (G) invasion capacity of A375 cells were strengthened after KCTD12 knockdown (24 h). Scale bars: 50 μm. Data are mean ± SD (n = 3 - 5); *, $P < 0.05$; **, $P < 0.01$, determined by one-tailed unpaired t-test.

Depressed KCTD12 expression enhances the stemness of melanoma cells

Under normal physiological conditions, melanoma B16F10 cells synthesize and secrete a good deal of melanin[44]. However, we found a far lighter colored cell pellet after B16F10 cells were treated with KCTD12-siRNA (**Figure 4A**, left panel). Further experiments showed that the melanin content decreased to less than 40% in KCTD12 knockdown cells when compared with that in control cells (**Figure 4A**, middle panel; $P < 0.01$). In addition, the tyrosinase activity of KCTD12 knockdown B16F10 cells also decreased to approximately 40% when compared with that of control cells (**Figure 4A**, right panel; $P < 0.01$). Moreover, the melanin biosynthesis pathway related genes tyrosinase (*TYR*), 5,6-dihydroxyindole-2-carboxylic acid oxidase (*TYRP1*) and L-dopachrome tautomerase (*DCT*) were downregulated dramatically at the transcriptional level after KCTD12 knockdown (**Figure 4C**, first panel). As melanogenesis is a marker of melanoma cell differentiation[45], dedifferentiated melanoma cells always have reduced melanin production[11]. Hence, we hypothesized that the aggressive biological behavior acquired by KCTD12 knockdown resulted from the dedifferentiation of melanoma cells. As evidence of dedifferentiation in KCTD12 knockdown/knockout cells, the expression of the melanoma cell differentiation marker microphthalmia-associated transcription factor (*MITF*), was significantly downregulated (**Figure 4C**, first panel and **Supplementary Figure S10**; $P < 0.01$).

Because dedifferentiation was reported to be associated

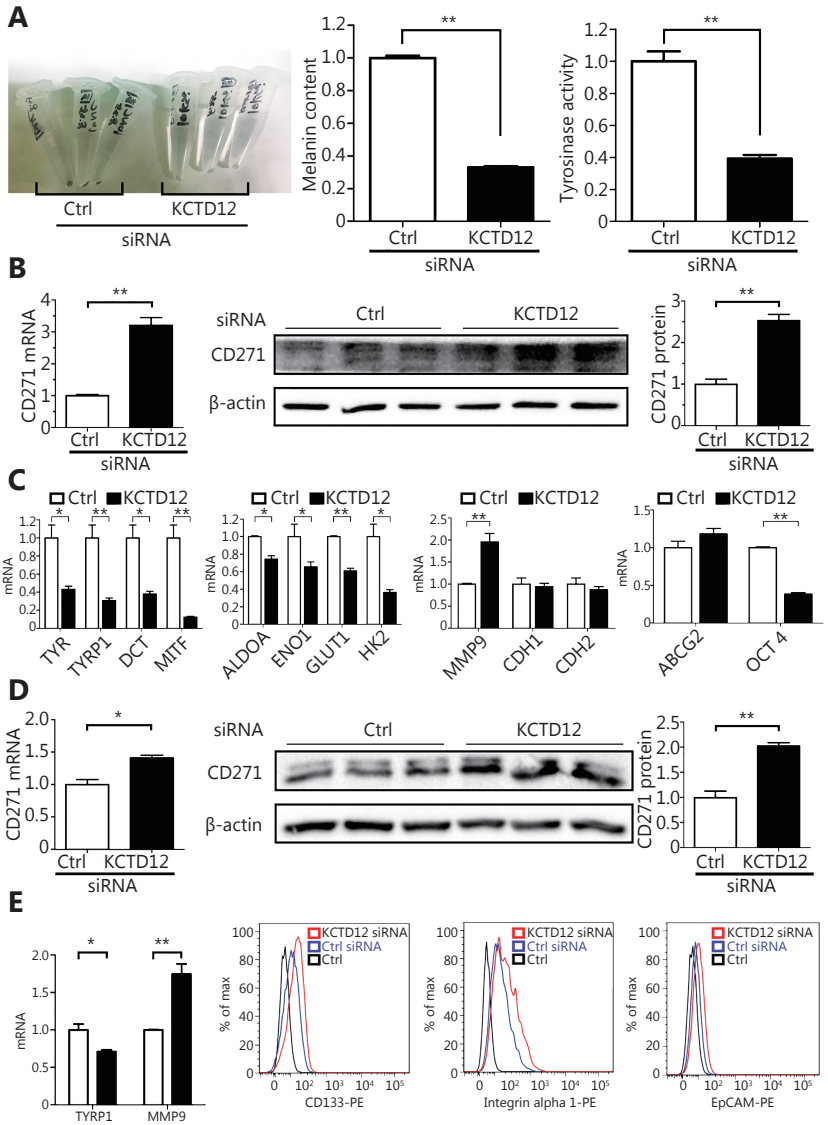

Figure 4 KCTD12 knockdown endows B16F10 and A375 cells the CSC-like traits. (A) KCTD12 knockdown decreased B16F10 cells' melanogenesis and the corresponding tyrosinase activity. (B) The upregulation of melanoma CSC marker CD271 was confirmed by RT-qPCR (left panel) and Western blot (middle and right panels) after KCTD12 knockdown in B16F10. (C) Expression of genes associated with melanogenesis, glycolysis, invasion, EMT, differentiation and CSC after KCTD12 knockdown in B16F10 were detected by RT-qPCR. (D) The upregulation of melanoma CSC marker CD271 was confirmed by RT-qPCR (left panel) and Western blot (middle and right panels) upon KCTD12 knockdown in A375. (E) Genes related to melanogenesis, CSC, adhesion, and invasion were detected after KCTD12 knockdown in A375 by RT-qPCR and FACS. Data are mean ± SD (n = 3 - 5); *, $P < 0.05$; **, $P < 0.01$, determined by one-tailed unpaired t-test.

with CSC transformation, we sought to determine whether KCTD12 knockdown-mediated dedifferentiation endowed melanoma cells with stemness. It has been reported that *CD271*, ATP-binding cassette sub-family G member 2 (*ABCG2*) and POU domain, class 5, *CD133*, transcription factor 1 (*OCT-4*), ATP-binding cassette sub-family B member 5 (ABCB5), Homeobox protein NANOG (Nanog) et al. are potential CSC markers[17,29,46,47]. Hence, we examined the expression of these genes in melanoma cells after KCTD12 knockdown/knockout. One of the MSC markers, CD271, was significantly upregulated at the transcriptional and translational levels in both B16F10 cells (**Figure 4B**; $P < 0.01$) and A375 cells (**Figure 4D**; $P < 0.05$) after KCTD12 knockdown. In addition to melanoma cells, the upregulation of CD271 was also observed in lung cancer A549 cells after KCTD12 knockdown (**Supplementary Figure S11**).

Moreover, flow cytometry analysis indicated that CD133 was increased slightly in A375 cells after KCTD12 knockdown (**Figure 4E**, second panel). In addition, other CSC markers, *ABCB5*, *ALDH1A1*, *JARID1B*, *JUN*, *KLF4* and *Nanog*, were all observed upregulation in the transcriptional level after KCTD12 knockout in A375 cells (**Supplementary Figure S12**). The transcription of the *ABCG2* gene was also increased mildly but nonsignificantly (**Figure 4C**, fourth panel; $P > 0.05$). Strangely, the known MSC marker, *OCT-4*[17], was downregulated at the transcriptional level (**Figure 4C**, fourth panel; $P < 0.01$).

Because stem cell transformation might involve EMT[48-50], we examined the expression of the EMT markers E-cadherin (*CDH1*) and N-cadherin (*CDH2*) in B16F10 and A375 cells after KCTD12 knockdown by RT-qPCR and Western blot. However, the results showed that the MSC transformation was independent of the known EMT process because E-cadherin and N-cadherin were not significantly changed at the mRNA level (**Figure 4C**, third panel; $P > 0.05$) or the protein level (**Supplementary Figure S13**; $P > 0.05$). Moreover, previous studies reported the involvement of ERK pathway in colorectal cancer stemness[5], so we examined the expression of ERK and p-ERK *via* Western blot. As shown in **Supplementary Figure S14**, KCTD12 downregulation hardly influence the expression of ERK and p-ERK. According to earlier reports, low MITF expression was related to the stemness in melanoma[51]. Hence, a MITF inhibitor was employed to examine the effect of MITF on CD271. As shown in **Supplementary Figure S10**, MITF downregulation increased the transcription level of CD271. In addition, the clinical data showed that MITF was reversely correlated with CD271 (**Supplementary Figure S10**).

Metabolism recombination after KCTD12 knockdown favors the assumption of MSC transformation

As previous studies reported[52-55], CSCs may depend more on oxidative phosphorylation (OXPHOS) and less on glycolysis for energy supply. In this study, we examined the mRNA expression of glycolysis-related genes. Fructose-bisphosphate aldolase A (*ALDOA*; $P < 0.05$), alpha-enolase (*ENO1*; $P < 0.05$), solute carrier family 2, facilitated glucose transporter member 1 (*GLUT1*; $P < 0.01$) and hexokinase-2 (*HK2*; $P < 0.05$) were downregulated significantly after KCTD12 knockdown in B16F10 cells (**Figure 4C**, second panel). These results strengthened the MCS transformation assumption.

Enhancing stemness increases melanoma cell spheroid formation capability and survival in a hostile environment

To further investigate the effects of KCTD12 loss on cell functions, KCTD12 was knocked out with the Clustered Regularly Interspaced Short Palindromic Repeats system (CRISPR/Cas9; **Figure 5A**; $P < 0.01$). Similar to the above results, KCTD12 knockout in A375 cells enhanced the expression of CD271 (**Figure 5A**; $P < 0.01$). We next examined the stress tolerance capacity and spheroid formation capacity after KCTD12 knockout in A375 cells. As shown in **Figure 5B**, after culture in basal medium without FBS supplementation for 4 days, the number of apoptotic cells in the KCTD12 knockout (KCTD12-KO) group was far less than that in the control group ($P < 0.01$). In the spheroid formation assay, equal amounts of cells were added to the spheroid microplates, and the size of the spheroids was monitored every day. The results showed that cell spheroids were much larger in the KCTD12-KO group than in the control group on the eighth day (1979 ± 45 μm *vs.* 1718 ± 32 μm for the diameter, respectively; $P < 0.01$), which indicated that KCTD12 knockout strengthened the A375 cells' spheroid formation capacity (**Figure 5C** and **Supplementary Figure S15**). Next, we examined the hypoxia tolerance of A375 cells before and after KCTD12 knockout using a calcein-AM/PI kit. The results showed that the hypoxia tolerance was greatly increased after KCTD12 knockout in A375 cells (**Figure 5D**; $P < 0.01$). Afterward, we detected the uptake and cytotoxicity of doxorubicin (DOX) in A375 cells before and after KCTD12 knockout with fluorography and MTT assays, respectively (**Figure 5E** and **5F**). The fluorescent photographs showed a dramatic reduction in DOX uptake in the KCTD12-KO group compared with that in the control group (**Figure 5E**). As a result, the half maximal inhibitory concentration (IC_{50}) values of DOX in the KCTD12-KO and control cells were 3.79 μg/mL and 1.83 μg/mL, respectively (**Figure 5F**), which suggested that KCTD12-KO cells were less sensitive to DOX than the control cells. Together, these results indicated that KCTD12 knockout-mediated stemness transformation increased melanoma cell spheroid formation capability and survival in a hostile environment.

Enhancing stemness promotes the metastasis of melanoma cells *in vivo*

To examine the effects of KCTD12 knockout-mediated

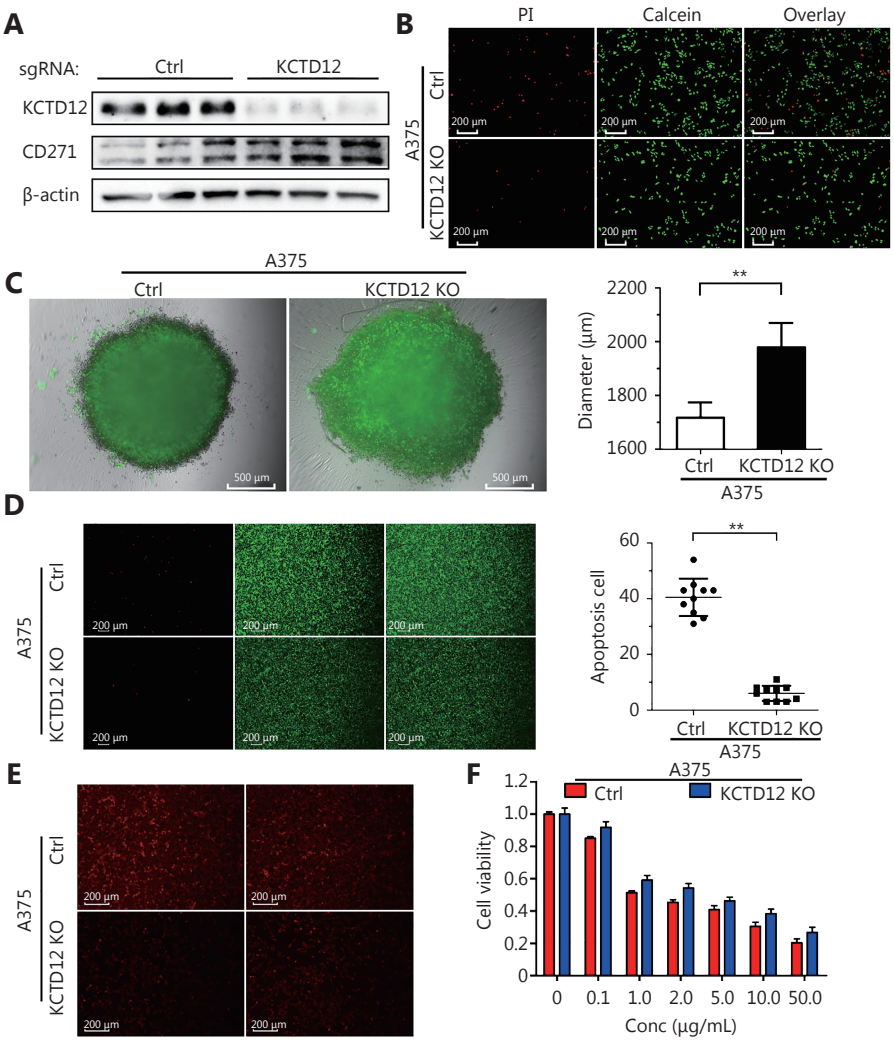

Figure 5 KCTD12 knockout enhances A375 cells' spheroids forming capacity and survival capacity in hostile environment. (A) KCTD12 knockout by CRISPR/Cas9, along with upregulation of CD271, was confirmed by Western blot. (B) Apoptotic cells were decreased in A375 cells after KCTD12 knockout when cultured in the basal medium without FBS for 8 days detected by Calcein-AM/PI kit. Scale bars: 200 μm. (C) KCTD12 knockout enhanced A375 cells' spheroids forming ability (8 days). Scale bars: 500 μm. (D) Apoptotic cells were decreased in A375 cells after KCTD12 knockout when cultured under a hypoxia condition for 4 days detected by Calcein-AM/PI kit. Scale bars: 200 μm. (E) KCTD12 knockout decreased the doxorubicin uptake in A375 cells (24 h). Scale bars: 200 μm. (F) KCTD12 knockout reduced the cytotoxicity of doxorubicin to A375 cells (24 h). Data are mean ± SD (n = 3 - 5); **, P < 0.01, determined by one-tailed unpaired t-test.

stemness transformation on metastasis *in vivo*, the same amount (2×10^6 cells) of A375 cells and A375-KCTD12-KO cells were injected intravenously into BALB/C nude mice (n = 4 per group). Nearly two months later, the mice were euthanized, and the major organs were collected for histological examination. As shown in **Figure 6A**, the body weights of the mice in two groups were not significantly different ($P > 0.05$). However, the metastatic burden was much greater in A375-KCTD12-KO cell-injected mice than in A375 cell-injected mice (**Figure 6B-6D**). Mice in the A375 cell-injected group did not develop macroscopic metastasis in their main organs (**Figure 6B-6C**). However, metastatic nodes were found in the liver, spleen and lungs of A375-KCTD12-KO cell-injected mice, and the metastatic ratios were 25% (1/4), 25% (1/4) and 100% (4/4), respectively (**Figure 6B-6C**). H&E staining confirmed the metastases in A375-KCTD12-KO cell-injected mice (**Figure 6D**). Taken together, these results indicated that KCTD12 knockout-mediated stemness transformation promotes the metastasis of melanoma cells *in vivo*.

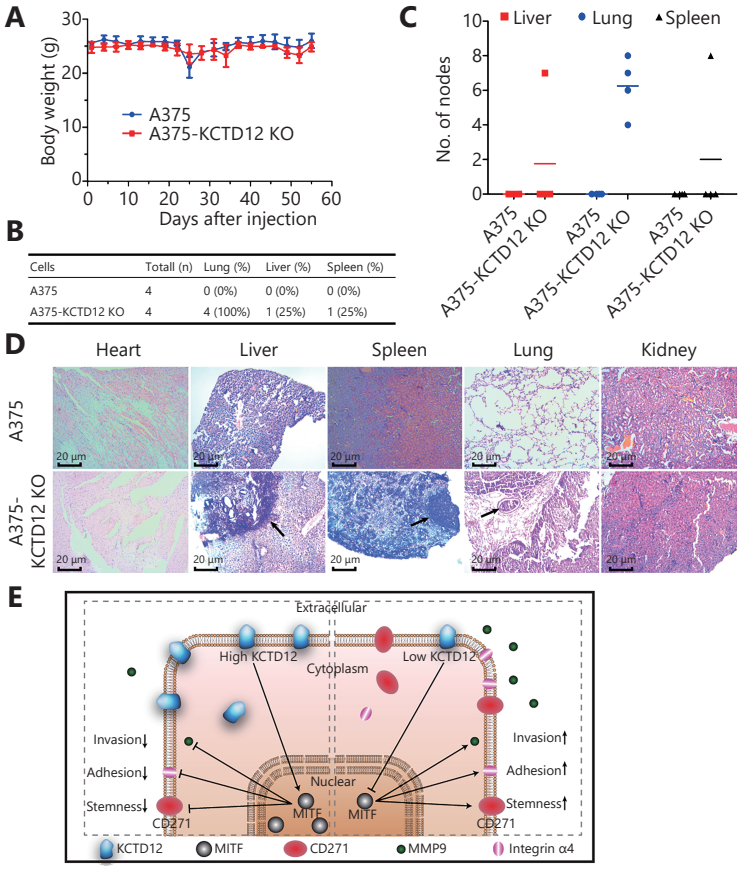

Cells	Totall (n)	Lung (%)	Liver (%)	Spleen (%)
A375	4	0 (0%)	0 (0%)	0 (0%)
A375-KCTD12 KO	4	4 (100%)	1 (25%)	1 (25%)

Figure 6 Knockout of KCTD12 promotes the metastasis of melanoma cells *in vivo*, and the schematic illustration of the potential mechanism. (A) Body weight changes of the mice (n = 4 per group) intravenously injected with A375 and A375-KCTD12-KO cells (2×10^6 per mouse). (B) The visceral metastasis rate of mice injected with A375 and A375-KCTD12-KO cell lines. (C) Statistical analysis of the metastatic nodes in the visceras. (D) H&E staining of the main viscera from the two groups. (E) Schematic illustration of the potential mechanism by which KCTD12 downregulation promotes melanoma metastasis.

Discussion

In the present study, we showed that KCTD12 was downregulated in metastatic melanoma cells, and KCTD12 expression was positively correlated with prognosis in SKCM patients. Our results also showed that KCTD12 downregulation promoted the proliferation and metastasis of melanoma cells *in vitro* and *in vivo*. We further demonstrated that KCTD12 knockout increased melanoma cell survival in a hostile environment. Moreover, we found the involvement of stemness transformation in KCTD12 downregulation-mediated metastasis.

Our proteomics results showed that KCTD12 was downregulated in metastatic melanoma cells compared with primary melanoma cells. Moreover, earlier reports showed that KCTD12 was downregulated in CSC-like colorectal cancer (CRC), and the decreased expression of KCTD12 was an independent prognostic factor for poor overall and disease-free survival in CRC patients[5]. In addition, KCTD12 was widely reported to be downregulated in gastrointestinal stromal tumors (GISTs) and served as a powerful prognostic marker for GISTs[56]. However, few studies have focused on the role of KCTD12 in melanoma metastasis[6]. In the present study, we analyzed the correlation between KCTD12 expression levels and the clinical prognosis of SKCM patients using the GEPIA database. The results indicated that KCTD12 acted as a positive prognostic factor in SKCM patients.

Our study also showed that KCTD12 downregulation significantly increased the growth, adhesion, migration and invasion of melanoma cells *in vitro* and *in vivo*. Moreover, we found that KCTD12 knockout increased the survival of melanoma cells in a hostile environment, such as hypoxia and starvation conditions. The underlying mechanism

through which KCTD12 downregulation promoted metastasis was preliminarily investigated. KCTD12 has been reported to suppress uveal melanoma cell proliferation by prolonging G2/M to G1 phase progression[6]. Earlier reports stated that KCTD12 inhibited CRC stemness and metastasis through suppressing the ERK pathway[5]. The latest study found that KCTD12 exerted its inhibitory role in ESCC through inhibiting stem cell factors[7]. However, the CSC hypothesis in melanoma is controversial[12,15]. In the present study, we found that KCTD12 knockdown upregulated the CSC markers CD271 and CD133. However, MSC transformation was not dependent on the EMT process or the ERK pathway. Further study revealed that MITF was downregulated after silencing KCTD12. It has been reported that MITF downregulation, along with CD271 upregulation, is involved in the acquisition of stemness in melanoma[51]. Furthermore, a previous study found that the $CD271^+$ population was enriched in low MITF expression melanoma cells[57]. In addition, the present study found MITF downregulation increased the transcription of CD271. Clinical data from GEPIA also showed that MITF was reversely correlated with CD271. Together, these data demonstrated that the main role of KCTD12 downregulation in promoting melanoma metastasis was attributed, at least partly, to MITF downregulation-mediated MSC transformation.

Conclusions

Overall, the present study reported that the loss of KCTD12 promoted melanoma metastasis by conferring anoikis-resistant ability and enhancing stemness. These results also provide a potential therapeutic target for the prevention of melanoma metastasis. However, further studies should be performed to determine the underlying regulatory mechanism of the KCTD12-MITF-CD271 axis in MSC transformation and metastasis.

Acknowledgments

The authors are grateful to Ms. Tingting Lv for the supply of pEGFP-N1 plasmid. This work was supported by grants from the Ministry of Science and Technology of China (Grant No. 2015CB931804), National Natural Science Foundation of China (Grant No. U1505225, 81773063, 81273548, 81571802), the Natural Science Foundation of Fujian Province (Grant No. 2016J06020), Fujian Development and Reform Commission project (Grant No. 829054).

Conflict of interest statement

No potential conflicts of interest are disclosed.

References

1. Kubota D, Orita H, Yoshida A, Gotoh M, Kanda T, Tsuda H, et al. Pfetin as a prognostic biomarker for gastrointestinal stromal tumor: validation study in multiple clinical facilities. Jpn J Clin Oncol. 2011; 41: 1194-202.
2. Kikuta K, Gotoh M, Kanda T, Tochigi N, Shimoda T, Hasegawa T, et al. Pfetin as a prognostic biomarker in gastrointestinal stromal tumor: novel monoclonal antibody and external validation study in multiple clinical facilities. Jpn J Clin Oncol. 2010; 40: 60-72.
3. Hasegawa T, Asanuma H, Ogino J, Hirohashi Y, Shinomura Y, Iwaki H, et al. Use of potassium channel tetramerization domain-containing 12 as a biomarker for diagnosis and prognosis of gastrointestinal stromal tumor. Hum Pathol. 2013; 44: 1271-7.
4. Kubota D, Okubo T, Saito T, Suehara Y, Yoshida A, Kikuta K, et al. Validation study on pfetin and ATP-dependent RNA helicase DDX39 as prognostic biomarkers in gastrointestinal stromal tumour. Jpn J Clin Oncol. 2012; 42: 730-41.
5. Li LP, Duan TM, Wang X, Zhang RH, Zhang MF, Wang SH, et al. KCTD12 regulates colorectal cancer cell stemness through the ERK pathway. Sci Rep. 2016; 6: 20460.
6. Luo LF, Cui JZ, Feng ZT, Li YN, Wang MD, Cai Y, et al. Lentiviral-mediated overexpression of KCTD12 inhibits the proliferation of human uveal melanoma OCM-1 cells. Oncol Rep. 2017; 37: 871-8.
7. Abbaszadegan MR, Taghehchian N, Li LP, Aarabi A, Moghbeli M. Contribution of KCTD12 to esophageal squamous cell carcinoma. BMC Cancer. 2018; 18: 853.
8. Ponti D, Costa A, Zaffaroni N, Pratesi G, Petrangolini G, Coradini D, et al. Isolation and *in vitro* propagation of tumorigenic breast cancer cells with stem/progenitor cell properties. Cancer Res. 2005; 65: 5506-11.
9. Eramo A, Lotti F, Sette G, Pilozzi E, Biffoni M, Di Virgilio A, et al. Identification and expansion of the tumorigenic lung cancer stem cell population. Cell Death Differ. 2008; 15: 504-14.
10. Ho MM, Ng AV, Lam S, Hung JY. Side population in human lung cancer cell lines and tumors is enriched with stem-like cancer cells. Cancer Res. 2007; 67: 4827-33.
11. Fang D, Nguyen TK, Leishear K, Finko R, Kulp AN, Hotz S, et al. A tumorigenic subpopulation with stem cell properties in melanomas. Cancer Res. 2005; 65: 9328-37.
12. Quintana E, Shackleton M, Foster HR, Fullen DR, Sabel MS, Johnson TM, et al. Phenotypic heterogeneity among tumorigenic melanoma cells from patients that is reversible and not hierarchically organized. Cancer Cell. 2010; 18: 510-23.
13. Pisanu ME, Maugeri-Saccà M, Fattore L, Bruschini S, De Vitis C, Tabbì E, et al. Inhibition of stearoyl-CoA desaturase 1 reverts BRAF and MEK inhibition-induced selection of cancer stem cells in BRAF-mutated melanoma. J Exp Clin Cancer Res. 2018; 37: 318.

14. Quintana E, Shackleton M, Sabel MS, Fullen DR, Johnson TM, Morrison SJ. Efficient tumour formation by single human melanoma cells. Nature. 2008; 456: 593-8.
15. Monzani E, Facchetti F, Galmozzi E, Corsini E, Benetti A, Cavazzin C, et al. Melanoma contains CD133 and ABCG2 positive cells with enhanced tumourigenic potential. Eur J Cancer. 2007; 43: 935-46.
16. Zabierowski SE, Herlyn M. Melanoma stem cells: the dark seed of melanoma. J Clin Oncol. 2008; 26: 2890-4.
17. Kumar SM, Liu S, Lu H, Zhang H, Zhang PJ, Gimotty PA, et al. Acquired cancer stem cell phenotypes through oct4-mediated dedifferentiation. Oncogene. 2012; 31: 4898-911.
18. Thiery JP, Acloque H, Huang RYJ, Nieto MA. Epithelial-mesenchymal transitions in development and disease. Cell. 2009; 139: 871-90.
19. Herreros-Villanueva M, Zhang JS, Koenig A, Abel EV, Smyrk TC, Bamlet WR, et al. SOX2 promotes dedifferentiation and imparts stem cell-like features to pancreatic cancer cells. Oncogenesis. 2013; 2: e61.
20. Yang MH, Hsu DSS, Wang HW, Wang HJ, Lan HY, Yang WH, et al. Bmi1 is essential in twist1-induced epithelial-mesenchymal transition. Nat Cell Biol. 2010; 12: 982-92.
21. Zhang MM, Miao F, Huang R, Liu WJ, Zhao YC, Jiao T, et al. RHBDD1 promotes colorectal cancer metastasis through the wnt signaling pathway and its downstream target ZEB1. J Exp Clin Cancer Res. 2018; 37: 22.
22. Friedmann-Morvinski D, Verma IM. Dedifferentiation and reprogramming: origins of cancer stem cells. EMBO Rep. 2014; 15: 244-53.
23. Zhang HX, Wu HT, Zheng JH, Yu P, Xu LX, Jiang P, et al. Transforming growth factor β1 signal is crucial for dedifferentiation of cancer cells to cancer stem cells in osteosarcoma. Stem Cells. 2013; 31: 433-46.
24. Civenni G, Walter A, Kobert N, Mihic-Probst D, Zipser M, Belloni B, et al. Human CD271-positive melanoma stem cells associated with metastasis establish tumor heterogeneity and long-term growth. Cancer Res. 2011; 71: 3098-109.
25. Shakhova O, Sommer L. Testing the cancer stem cell hypothesis in melanoma: the clinics will tell. Cancer Lett. 2013; 338: 74-81.
26. Murillo-Sauca O, Chung MK, Shin JH, Karamboulas C, Kwok S, Jung YH, et al. CD271 is a functional and targetable marker of tumor-initiating cells in head and neck squamous cell carcinoma. Oncotarget. 2014; 5: 6854-66.
27. Wirths S, Malenke E, Kluba T, Rieger S, Müller MR, Schleicher S, et al. Shared cell surface marker expression in mesenchymal stem cells and adult sarcomas. Stem Cells Transl Med. 2013; 2: 53-60.
28. Huang SD, Yuan Y, Liu XH, Gong DJ, Bai CG, Wang F, et al. Self-renewal and chemotherapy resistance of $p75^{NTR}$ positive cells in esophageal squamous cell carcinomas. BMC Cancer. 2009; 9: 9.
29. Boiko AD, Razorenova OV, van de Rijn M, Swetter SM, Johnson DL, Ly DP, et al. Human melanoma-initiating cells express neural crest nerve growth factor receptor CD271. Nature. 2010; 466: 133-7.
30. Wang JC, Chen JZ, Zhu YW, Zheng N, Liu J, Xiao YY, et al. *In vitro* and *in vivo* efficacy and safety evaluation of metapristone and mifepristone as cancer metastatic chemopreventive agents. Biomed Pharmacother. 2016; 78: 291-300.
31. Shi Q, Jiang Z, Yang JY, Cheng YL, Pang YQ, Zheng N, et al. A flavonoid glycoside compound from *Murraya paniculata* (L.) interrupts metastatic characteristics of A549 cells by regulating STAT3/NF-κB/COX-2 and EGFR signaling pathways. AAPS J. 2017; 19: 1779-90.
32. Liu M, Wang YY, Ruan YX, Bai CS, Qiu L, Cui YF, et al. PKM2 promotes reductive glutamine metabolism. Cancer Bio Med. 2018; 15: 389-99.
33. Zheng N, Chen JH, Li T, Liu WQ, Liu J, Chen HN, et al. Abortifacient metapristone (RU486 derivative) interrupts CXCL12/CXCR4 axis for ovarian metastatic chemoprevention. Mol Carcinog. 2017; 56: 1896-908.
34. Lu YS, Liang HY, Yu T, Xie JJ, Chen SM, Dong HY, et al. Isolation and characterization of living circulating tumor cells in patients by immunomagnetic negative enrichment coupled with flow cytometry. Cancer. 2015; 121: 3036-45.
35. Dong HY, Han LY, Wu ZS, Zhang T, Xie JJ, Ma J, et al. Biostable aptamer rings conjugated for targeting two biomarkers on circulating tumor cells *in vivo* with great precision. Chem Mater. 2017; 29: 10312-25.
36. Jiang K, Chi T, Li T, Zheng GR, Fan LL, Liu YJ, et al. A smart pH-responsive nano-carrier as a drug delivery system for the targeted delivery of ursolic acid: suppresses cancer growth and metastasis by modulating P53/MMP-9/PTEN/CD44 mediated multiple signaling pathways. Nanoscale. 2017; 9: 9428-39.
37. Zheng GR, Shen ZC, Chen HN, Liu J, Jiang K, Fan LL, et al. Metapristone suppresses non-small cell lung cancer proliferation and metastasis *via* modulating RAS/RAF/MEK/MAPK signaling pathway. Biomed Pharmacother. 2017; 90: 437-45.
38. Fu QH, Zhang Q, Lou Y, Yang JQ, Nie G, Chen Q, et al. Primary tumor-derived exosomes facilitate metastasis by regulating adhesion of circulating tumor cells *via* SMAD3 in liver cancer. Oncogene. 2018; 37: 6105-18.
39. Zheng N, Chen JH, Liu WQ, Wang JC, Liu J, Jia L. Metapristone (RU486 derivative) inhibits cell proliferation and migration as melanoma metastatic chemopreventive agent. Biomed Pharmacother. 2017; 90: 339-49.
40. Asangani IA, Rasheed SAK, Nikolova DA, Leupold JH, Colburn NH, Post S, et al. MicroRNA-21 (miR-21) post-transcriptionally downregulates tumor suppressor pdcd4 and stimulates invasion, intravasation and metastasis in colorectal cancer. Oncogene. 2008; 27: 2128-36.
41. Zhao LM, Li J, Liu YP, Zhou W, Shan YN, Fan XY, et al. Flotillin1 promotes EMT of human small cell lung cancer *via* TGF-β signaling pathway. Cancer Bio Med. 2018; 15: 400-14.
42. Tang ZF, Li CW, Kang BX, Gao G, Li C, Zhang ZM. GEPIA: a web server for cancer and normal gene expression profiling and interactive analyses. Nucleic Acids Res. 2017; 45: W98-102.
43. Ran FA, Hsu PD, Wright J, Agarwala V, Scott DA, Zhang F. Genome engineering using the CRISPR-cas9 system. Nat Protoc.

2013; 8: 2281-308.

44. Kageyama A, Oka M, Okada T, Nakamura SI, Ueyama T, Saito N, et al. Down-regulation of melanogenesis by phospholipase D2 through ubiquitin proteasome-mediated degradation of tyrosinase. J Biol Chem. 2004; 279: 27774-80.
45. Bennett DC. Differentiation in mouse melanoma cells: initial reversibility and an on-off stochastic model. Cell. 1983; 34: 445-53.
46. Lee N, Barthel SR, Schatton T. Melanoma stem cells and metastasis: mimicking hematopoietic cell trafficking? Lab Invest. 2014; 94: 13-30.
47. Chiou SH, Yu CC, Huang CY, Lin SC, Liu CJ, Tsai TH, et al. Positive correlations of oct-4 and nanog in oral cancer stem-like cells and high-grade oral squamous cell carcinoma. Clin Cancer Res. 2008; 14: 4085-95.
48. Singh A, Settleman J. EMT, cancer stem cells and drug resistance: an emerging axis of evil in the war on cancer. Oncogene. 2010; 29: 4741-51.
49. Polyak K, Weinberg RA. Transitions between epithelial and mesenchymal states: acquisition of malignant and stem cell traits. Nat Rev Cancer. 2009; 9: 265-73.
50. Mani SA, Guo WJ, Liao MJ, Eaton EN, Ayyanan A, Zhou AY, et al. The epithelial-mesenchymal transition generates cells with properties of stem cells. Cell. 2008; 133: 704-15.
51. Perotti V, Baldassari P, Molla A, Vegetti C, Bersani I, Maurichi A, et al. NFATc2 is an intrinsic regulator of melanoma dedifferentiation. Oncogene. 2016; 35: 2862-72.
52. Peiris-Pagès M, Martinez-Outschoorn UE, Pestell RG, Sotgia F, Lisanti MP. Cancer stem cell metabolism. Breast Cancer Res. 2016; 18: 55.
53. Ye XQ, Li Q, Wang GH, Sun FF, Huang GJ, Bian XW, et al. Mitochondrial and energy metabolism-related properties as novel indicators of lung cancer stem cells. Int J Cancer. 2011; 129: 820-31.
54. Janiszewska M, Suvà ML, Riggi N, Houtkooper RH, Auwerx J, Clément-Schatlo V, et al. Imp2 controls oxidative phosphorylation and is crucial for preserving glioblastoma cancer stem cells. Genes Dev. 2012; 26: 1926-44.
55. Sancho P, Burgos-Ramos E, Tavera A, Bou Kheir T, Jagust P, Schoenhals M, et al. MYC/PGC-1α balance determines the metabolic phenotype and plasticity of pancreatic cancer stem cells. Cell Metab. 2015; 22: 590-605.
56. Orita H, Ito T, Kushida T, Sakurada M, Maekawa H, Wada R, et al. Pfetin as a risk factor of recurrence in gastrointestinal stromal tumors. Biomed Res Int. 2014; 2014: 651935.
57. Cheli Y, Bonnazi VF, Jacquel A, Allegra M, De Donatis GM, Bahadoran P, et al. CD271 is an imperfect marker for melanoma initiating cells. Oncotarget. 2014; 5: 5272-83.

Cite this article as: Shen W, Li Y, Li B, Zheng L, Xie X, Le J, et al. Downregulation of KCTD12 contributes to melanoma stemness by modulating CD271. Cancer Biol Med. 2019; 16: 498-513. doi: 10.20892/j.issn.2095-3941.2019.0073

Supplementary materials

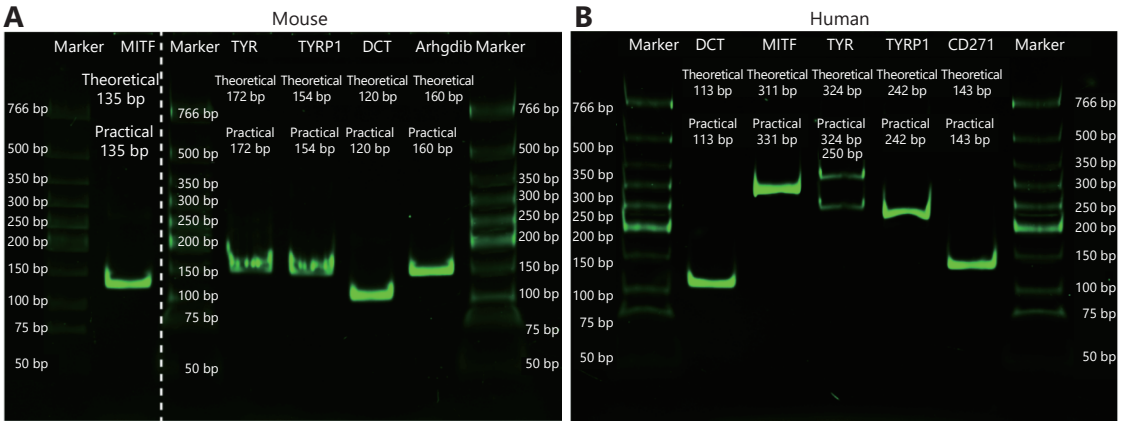

Figure S1 Verification of the RT-qPCR products by SDS-PAGE. (A) Bands of RT-qPCR products stained with SYBR green from mouse melanoma cells. (B) Bands of RT-qPCR products stained with SYBR green from human melanoma cells.

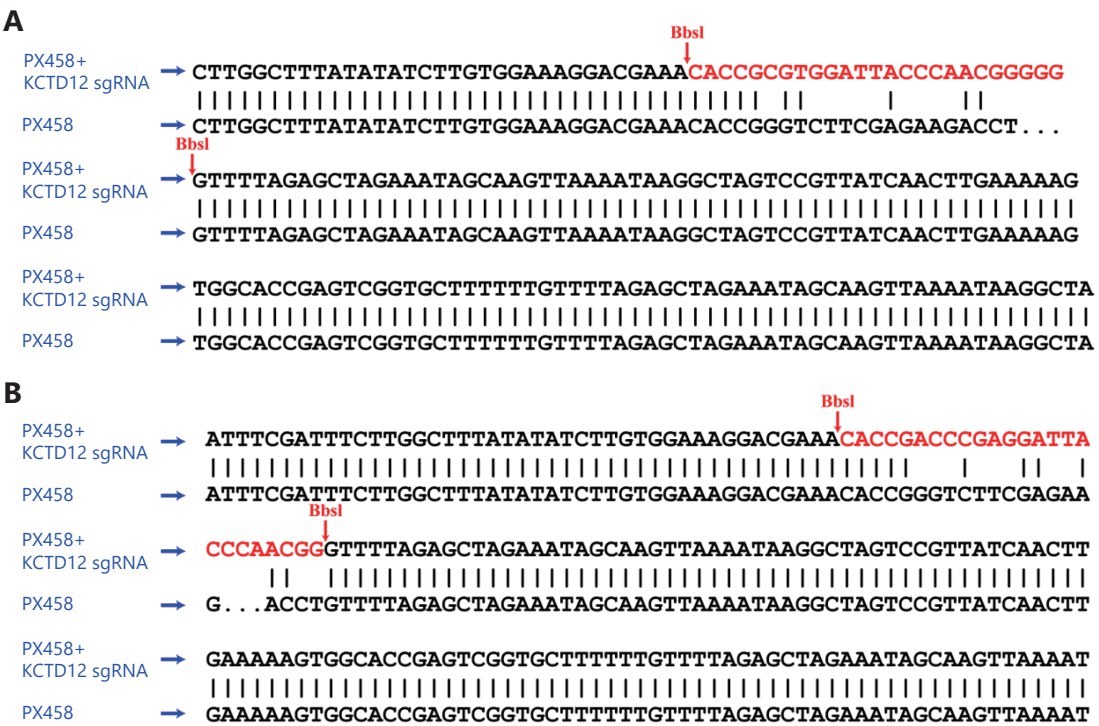

Figure S2 The construction of KCTD12 knockout CRISPR/Cas9 system was verified by sequencing. (A) The alignment result of PX458 plasmid with connect product formed by PX458 plasmid and sgRNA (A375). (B) The alignment result of PX458 plasmid with connect product formed by PX458 plasmid and sgRNA (B16F10).

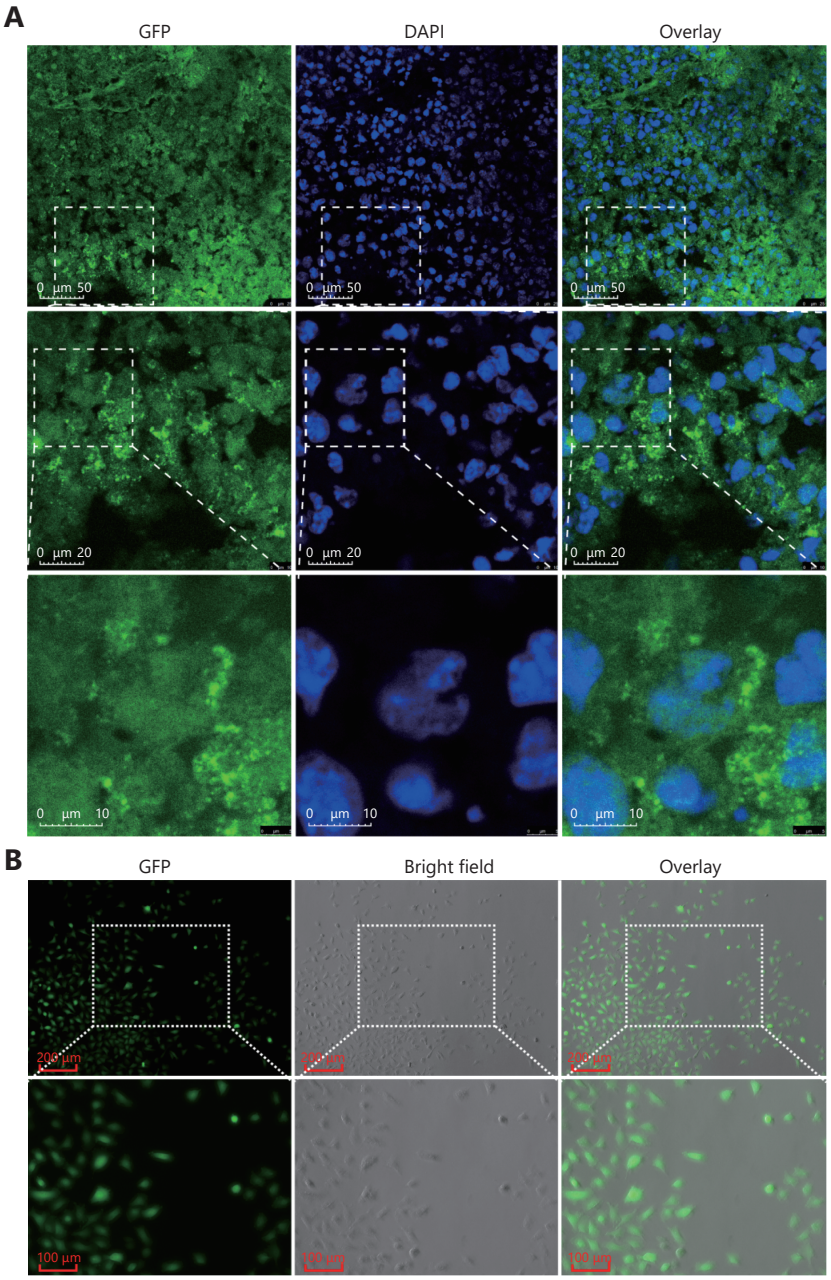

Figure S3 The establishment of A375M cell line was confirmed by fluorescence microphotography. (A) Laser scanning confocal microscope photographs of metastatic tumor sections in lung from BALB/C nude mouse after A375-GFP cells being injected for 2 months through caudal vein. Scale bars in the up, middle and low panel were 50 μm, 20 μm and 10 μm, respectively. (B) Fluorescence microphotography of the established A375M cell line. Scale bars in the up and low panel were 200 μm and 100 μm, respectively.

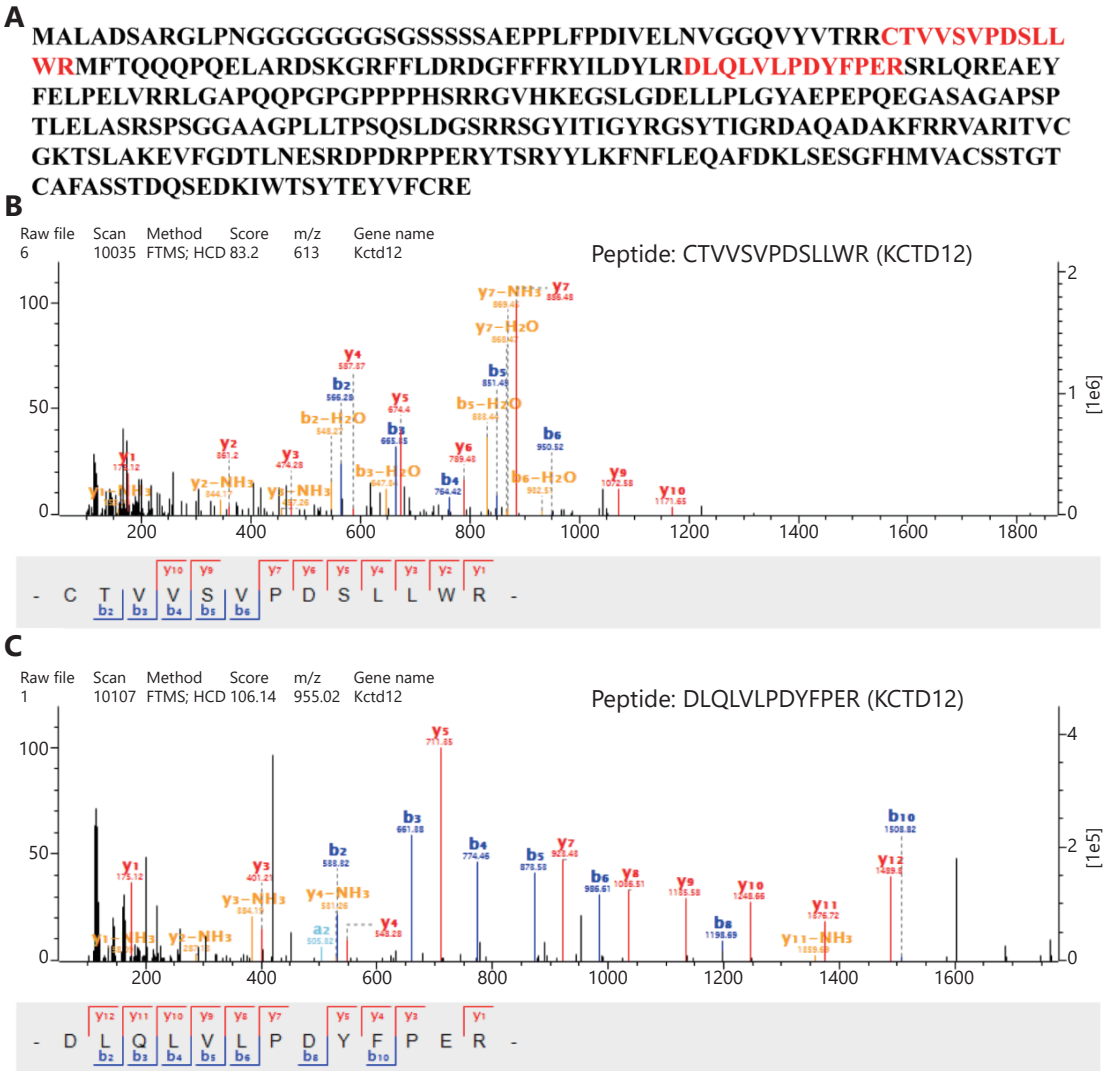

Figure S4 Identification of KCTD12 protein from two characteristic peptides in iTRAQ. (A) The amino acid sequence of protein KCTD12. (B, C) Two characteristic peptides identified in iTRAQ, CTVVSVPDSLLWR (B) and DLQLVLPDYFPER (C), were in keeping with two sequences in KCTD12 protein highlighted with red font in A.

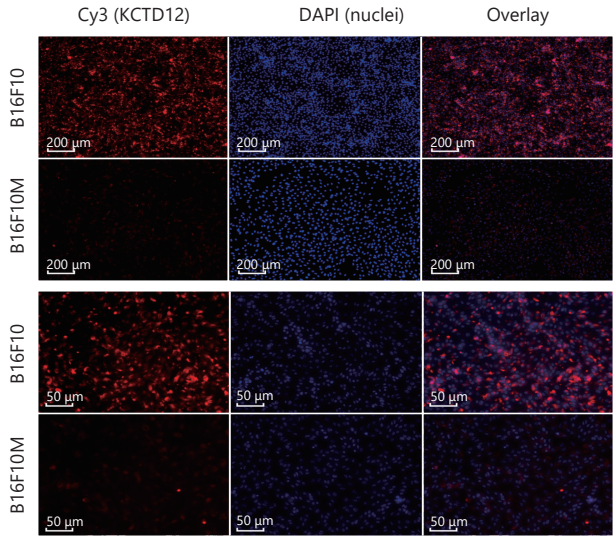

Figure S5 Lower KCTD12 levels in B16F10M cells than in parental B16F10 cells were confirmed by immunofluorescence. Red fluorescence intensity indicates the abundance of KCTD12, and blue fluorescence indicates the cell nucleus. Scale bars in the up and low panel were 200 μm and 50 μm, respectively.

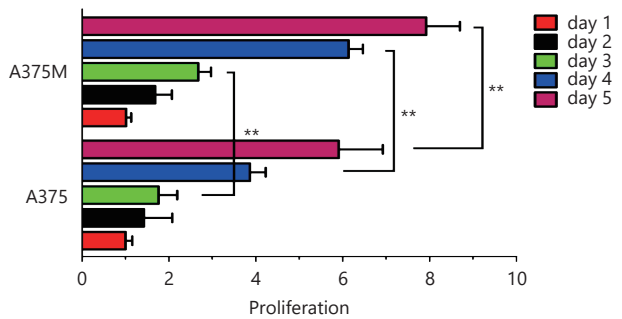

Figure S6 Proliferative capacity of A375M cells was higher than that of A375 cells. Data are mean ± s.d. (n = 3 - 5); **, P < 0.01, determined by one-tailed unpaired t-test.

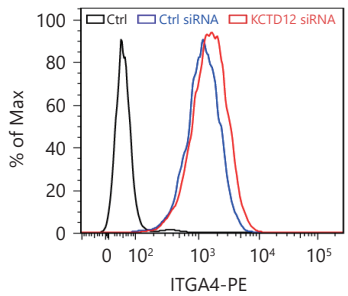

Figure S7 The upregulation of integrin alpha-4 (ITGA4) was verified by FACS after KCTD12 knockdown in B16F10 cells.

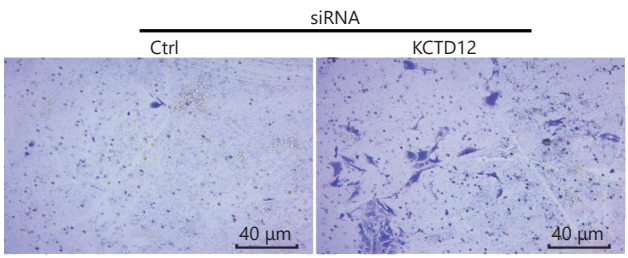

Figure S8 The elevated mobility of colon cancer SW620 cells was confirmed by transwell migration assay after KCTD12 knockdown (48 h).

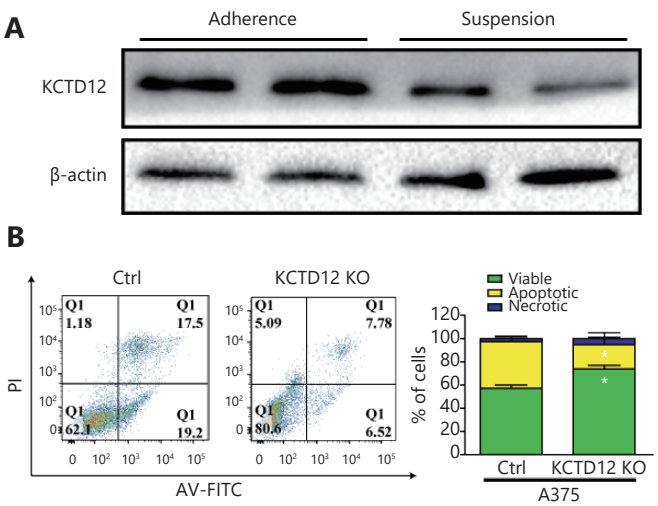

Figure S9 Low expression of KCTD12 confers A375 cells the anoikis-resistant ability. (A) The expression of KCTD12 in suspension cultured A375 cells was lower than that in adherent A375 cells. (B) The apoptotic ratio in A375-KCTD12-KO cells was lower than that in A375 cells when suspension culture for 1 day. Data are mean ± s.d. (n = 3 - 5); *, P < 0.05, determined by one-tailed unpaired t-test.

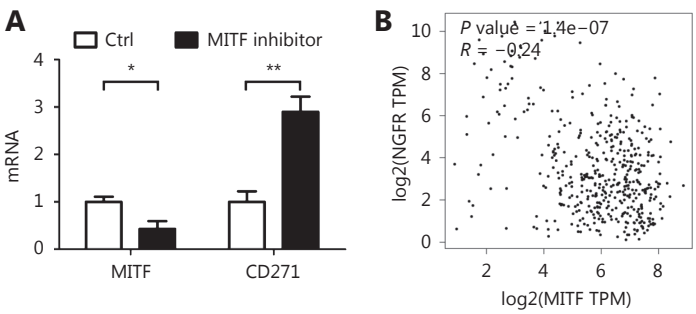

Figure S10 MITF was reversely correlated with CD271. (A) MITF downregulation increased the transcription level of CD271. (B) The inverse correlation between MITF and CD271 was confirmed by the clinical data. Data are mean ± s.d. (n = 3 - 5); *, P < 0.05; **, P < 0.01, determined by one-tailed unpaired t-test.

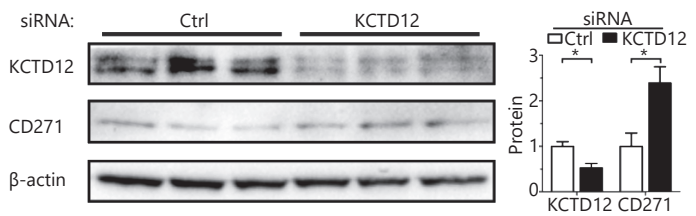

Figure S11 KCTD12 knockdown by siRNA, along with upregulation of CD271, was confirmed by western blot in A549 cells. Data are mean ± s.d. (n = 3 - 5); *, P < 0.05, determined by one-tailed unpaired t-test.

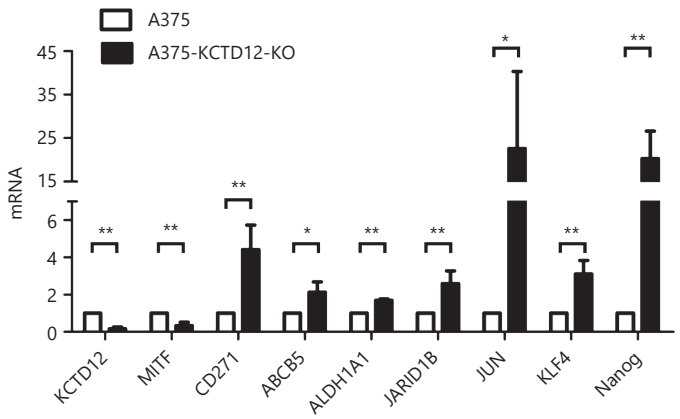

Figure S12 KCTD12 knockout decreased the transcriptional level of *MITF* and increased the transcriptional level of CSC genes in A375 cells. Data are mean ± s.d. (n = 3 - 5); *, P < 0.05; **, P < 0.01, determined by one-tailed unpaired t-test.

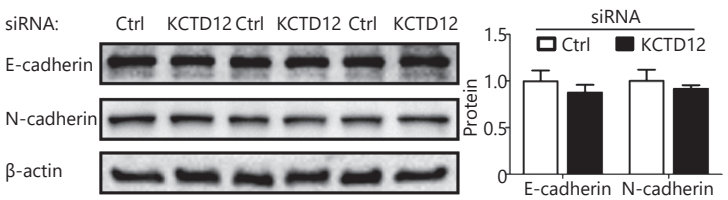

Figure S13 The expression difference of E-cadherin and N-cadherin was almost negligible after KCTD12 knockdown in A375 cells. Data are mean ± s.d. (n = 3 - 5).

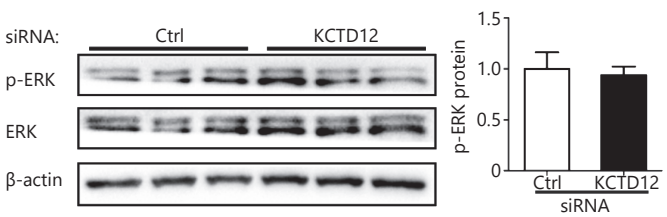

Figure S14 The expression difference of p-ERK was almost negligible before and after KCTD12 knockdown in A375 cells. Data are mean ± s.d. (n = 3 - 5).

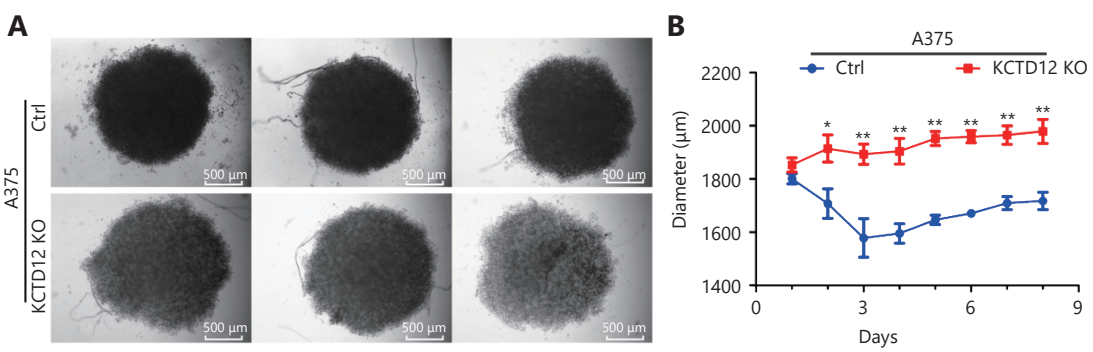

Figure S15 The elevated spheroid formation ability was confirmed by spheroid formation assay after KCTD12 knockout in A375 cells. (A) The photographs of spheroids formed by A375 cells and A375-KCTD12-KO cells at the eighth day. (B) The quantification of spheroid diameter from the first day to the eighth day. Data are mean ± s.d. (n = 3 - 5); *, P < 0.05; **, P < 0.01, determined by one-tailed unpaired t-test.

Table S1 RT-qPCR primers used in this study

Gene	Forward primer (5'-3')	Reverse primer (5'-3')
CD271[a]	CTAGGGGTGTCCTTTGGAGGT	CAGGGTTCACACACGGTCT
MMP-9[a]	CTGGACAGCCAGACACTAAAG	CTCGCGGCAAGTCTTCAGAG
ABCG2[a]	CTCAGTTTATCCGTGGCA	GACCCTGTTTAGACATCCTT
OCT4[a]	CGGAAGAGAAAGCGAACTAGC	ATTGGCGATGTGAGTGATCTG
CDH1[a]	AGGGACGGTCAACAACT	CACCTCCTTCTTCATCATAG
CDH2[a]	CTCCAGAACCCAACTCAA	CGCCGTTTCATCCATAC
CCND1[a]	GCGTACCCTGACACCAATCTC	CTCCTCTTCGCACTTCTGCTC
TYRP1[a]	ATACTGGGACCAGATGGCAACACA	AAGCGGGTCCTTCGTGAGAGAAAT
MITF[a]	TTGATGGATCCGGCCTTGCAAATG	TATGTTGGGAAGGTTGGCTGGACA
DCT[a]	CTAACCGCAGAGCAACTTGG	CAAGAGCAAGACGAAAGCTCC
TYR[a]	AGTCGTATCTGGCCATGGCTTCTT	ACAGCAAGCTGTGGTAGTCGTCTT
ACTB[a]	GGCTGTATTCCCCTCCATCG	CCAGTTGGTAACAATGCCATGT
KCTD12[b]	GCTCGGGCTACATCACCATC	GGTCCCGGCTTTCGTTCAG
MMP9[b]	GCACGACGTCTTCCAGTACC	TCAACTCACTCCGGGAACTC
CD271[b]	CGAGGCACCACCGACAACCT	TGGTTCACTGGCCGGCTGTT
DCT[b]	CTCAGACCAACTTGGCTACAGC	CAACCAAAGCCACCAGTGTTCC
TYRP1[b]	GGCTGTATCTTCTTCCCCTT	CAGACCTCCCGATCATCTCT
TYR[b]	TTTGTACTGCCTGCTGTGGA	TGTGCAGTTTGGTCCCCAA
MITF[b]	CGGGTCTCTGCTCTCCAGA	CCGGCTGCTTGTTTTGGAA
JUN[b]	TCTCACAAACCTCCCTCCTG	GAGGGGGTTACAAACTGCAA
ALDH1A1[b]	ACTGCTCTCCACGTGGCATCTTTA	TGCCAACCTCTGTTGATCCTGTGA
JARID1B[b]	AGTGCAGTGGCGCGATCT	GGCAGAAGAATTGCTGGAATCTAG
ABCB5[b]	CACAAAAGGCCATTCAGGCT	GCTGAGGAATCCACCCAATCT
Nanog[b]	CAGGTGTTTGAGGGTAGCTC	CGGTTCATCATGGTACAGTC
KLF4[b]	TGCTGATTGTCTATTTTTGCGTTTA	GAGAAGAAACGAAGCCAAAACC
ACTB[b]	AGAAAATCTGGCACCACACC	AGAGGCGTACAGGGATAGCA

NOTE.[a] is for mouse, and [b] is for human.

Table S2 siRNAs used in this study

Gene	Sense (5'-3')	Anti-sense (5'-3')
KCTD12	GCUACAUCACCAUCGGCUATT	UAGCCGAUGGUGAUGUAGCTT
NC	UUCUCCGAACGUGUCACGUTT	ACGUGACACGUUCGGAGAATT
FAM NC	UUCUCCGAACGUGUCACGUTT	ACGUGACACGUUCGGAGAATT
GAPDH	CACUCAAGAUUGUCAGCAATT	UUGCUGACAAUCUUGAGUGAG